Nagra
Nationale
Genossenschaft
für die Lagerung
radioaktiver Abfälle

Cédra
Société coopérative
nationale
pour l'entreposage
de déchets radioactifs

Cisra
Società cooperativa
nazionale
per l'immagazzinamento
di scorie radioattive

TECHNICAL REPORT 87-30

Crosshole Investigations – Short and Medium Range Seismic Tomography

Calin Cosma

Vibrometric OY, Finland

February 1987

Parkstrasse 23 5401 Baden/Schweiz Telephon 056/20 55 11

Nagra
Nationale
Genossenschaft
für die Lagerung
radioaktiver Abfälle

Cédra
Société coopérative
nationale
pour l'entreposage
de déchets radioactifs

Cisra
Società cooperativa
nazionale
per l'immagazzinamento
di scorie radioattive

TECHNICAL REPORT 87-30

Crosshole Investigations – Short and Medium Range Seismic Tomography

Calin Cosma

February 1987

Vibrometric OY, Finland

Parkstrasse 23 5401 Baden/Schweiz Telephon 056/20 55 11

Der vorliegende Bericht betrifft eine Studie, die für das Stripa-Projekt ausgeführt wurde. Die Autoren haben ihre eigenen Ansichten und Schlussfolgerungen dargestellt.Diese müssen nicht unbedingt mit denjenigen des Auftraggebers übereinstimmen.

Le présent rapport a été préparé pour le projet de Stripa. Les opinions et conclusions présentées sont celles des auteurs et ne correspondent pas nécessairement à ceux du client.

This report concerns a study which was conducted for the Stripa Project. The conclusions and viewpoints presented in the report are those of the authors and do not necessarily coincide with those of the client.

Das Stripa-Projekt ist ein Projekt der Nuklearagentur der OECD. Unter internationaler Beteiligung werden von 1980-86 Forschungsarbeiten in einem unterirdischen Felslabor in Schweden durchgeführt. Diese sollen die Kenntnisse auf folgenden Gebieten erweitern:
- hydrogeologische und geochemische Messungen in Bohrlöchern
- Ausbreitung des Grundwassers und Transport von Radionukliden durch Klüfte im Gestein
- Verhalten von Materialien, welche zur Verfüllung und Versiegelung von Endlagern eingesetzt werden sollen
- Methoden zur zerstörungsfreien Ortung von Störzonen im Fels

Seitens der Schweiz beteiligt sich die Nagra an diesen Untersuchungen. Die technischen Berichte aus dem Stripa-Projekt erscheinen gleichzeitig in der NTB-Serie der Nagra.

The Stripa Project is organised as an autonomous project of the Nuclear Energy Agency of the OECD. In the period from 1980-86, an international cooperative programme of investigations is being carried out in an underground rock laboratory in Sweden. The aim of the work is to improve our knowledge in the following areas:
- hydrogeological and geochemical measurement methods in boreholes
- flow of groundwater and transport of radionuclides in fissured rock
- behaviour of backfilling and sealing materials in a real geological environment
- non-destructive methods for location of disturbed zones in the rock

Switzerland is represented in the Stripa Project by Nagra and the Stripa Project technical reports appear in the Nagra NTB series.

Le projet Stripa est un projet autonome de l'Agence de l'OCDE pour l'Energie Nucléaire. Il s'agit d'un programme de recherche avec participation internationale, qui sera réalisé entre 1980 et 1986 dans un laboratoire souterrain, en Suède. Le but de ces travaux est d'améliorer et d'étendre les connaissances dans les domaines suivants:
- mesures hydrogéologiques et géochimiques dans les puits de forage
- chimie des eaux souterraines à grande profondeur
- écoulement des eaux souterraines et transport des radionucléides dans les roches fracturées
- comportement des matériaux de colmatage et de scellement des dépôt finals
- méthodes de localisation non destructive des zones de perturbation de la roche

La Suisse est représentée dans le projet Stripa par la Cédra. Les rapports techniques du projet Stripa sont publiés dans la série des rapports techniques de la Cédra (NTB).

ABSTRACT

Seismic tomographic tests were conducted as a part of the Crosshole Investigations program of the Stripa Project. The aim has been to study if it is possible to detect by seismic tomography major fracture zones and determine their dimensions and orientation. The analysis was based on both compressional (P) and transversal (S) waves. The Young's modulus has been also calculated for a sub-set of measurements as a cross check for the P and S wave velocities.

The experimental data was collected at the crosshole site in the Stripa mine during 1984-1985. A down-the-hole impact source was used together with triaxial detectors and a digital seismograph. Five tomographic sections were obtained. The number of records per section was appr. 250. Measurements were done down to 200 m depth in all boreholes.

The main conclusion of this report is that it is possible to detect major fracture zones by seismic tomography. Their position and orientation can also be estimated.

RESUME

Des tests de tomographie sismique ont été réalisés dans le cadre du programme d'investigations entre puits du projet de Stripa. Ils avaient pour objectif d'étudier si la tomographie sismique permet de détecter des zones de fractures majeures et de déterminer leurs dimensions et orientation. L'analyse se basait sur des ondes de compression (P) et des ondes transversales (S). Le module de Young a lui aussi été calculé pour un sous-ensemble de mesures, afin de permettre un contrôle avec les vitesses des ondes P et S.

De 1984 à 1985, les données expérimentales ont été recueillies dans la mine de Stripa, sur le site d'essais entre puits. On a utilisé une source d'impact au fond du trou de forage, ainsi que des détecteurs à trois axes et un sismographe digital. Cinque sections tomographiques ont ainsi été obtenues, chacune fournissant près de 250 enregistrements. Des mesures ont été réalisées dans tous les forages, jusqu'à une profondeur de 200 m.

Ce rapport permet de conclure que la tomographie sismique permet de détecter des zones de fractures majeures ainsi que d'estimer leur position et orientation.

ZUSAMMENFASSUNG

Im Rahmen des Crosshole-Untersuchungsprogramms wurden seismische Tomographie-Testmessungen durchgeführt. Ziel dieser Untersuchung war festzustellen, ob mit Hilfe der seismischen Tomographie grössere Störzonen geortet und Aussagen über die Mächtigkeit und die räumliche Lage der Diskontinuitäten gemacht werden können. Die Untersuchungen wurden sowohl mit Kompressions- (P) als auch mit Transversalwellen (S) durchgeführt. Für einen Teil der Daten wurde das Elastizitätsmodul (Young's modulus) ermittelt, als Rückbestätigung für die P- und S-Wellengeschwindigkeiten.

Die Felddaten wurden im Laufe der Jahren 1984 bis 1985 im Gebiet des Crosshole-Versuchs in der Stripa-Mine gemessen. Die Signal-Aufzeichnung erfolgte über Dreikomponentenseismometer und eine digitale Registrierapparatur; als Quelle diente ein mechanischer Bohrlochhammer. Fünf Tomographiesektionen mit je ca. 250 Seismogrammspuren wurden aufgezeichnet, wobei in allen Bohrungen bis zu einer Tiefe von 200 m gemessen wurde.

Die Hauptaussage dieses Berichtes ist die Feststellung, dass mit der seismischen Tomographie grössere Störungen gefunden und ihre Lage und Ausrichtung abgeschätzt werden können.

TABLE OF CONTENTS

SUMMARY

The crosshole seismic tests which are presented in this report were intended to test the capability of the tomographic technique, when applied to seismic velocities, to describe the orientation, dimensions and properties of fracture zones. One of the main differences between this approach and similar tests performed at the same site is the attempt to include in the interpretation both P and S wave velocities.

The tests were performed at the 'Crosshole Site' in six fan-like boreholes drilled from the end of a drift at level 360 m of the Stripa Mine. The pyramidal volume investigated was located in a granite mass crossed by sections of deformed and fractured rock. These sections exhibit lower overall mechanical strength and therefore lower seismic velocities than the surrounding rockmass.

The field procedure consisted of emitting pulse signals from a source placed at various depths in one borehole and detecting them by means of sensors moved step by step in the other five boreholes. Each of the five pairs of boreholes was treated as a bidimensional section through the rock volume, this being a typical set-up for crosshole tomographic surveys.

The source of signals was a mechanical device (hammer) clamped to the borehole, which produced shocks along the borehole axis. The polarization of the strain field in the rock near the source due to the transient stress along the borehole created an important amount of S waves.

The detection of the signals was achieved by triaxial accelerometric probes which were also clamped to the borehole. The signals were recorded by means of a digital seismograph and then transfered to a micro-computer for further processing.

The tomographic routine which was used for processing the seismic velocity information had been inplemented on a micro-computer and several alterations were done to the original SIRT algorithm in order to increase the processing speed and to supress possible errors in the input data.

In spite of the very low velocity contrast between 'intact' and 'altered' rock, the main features were detected and their position is consistent in all sections used for interpretation. A remarcably good fit was obtained between the P and S velocity reconstructions of the same sections. The parallel processing of P and S velocities, if amounting like in this case to concordant results, adds confidence to the interpretation and also gives the means to estimate elastic parameters. Some values of the dynamic Young's modulus were calculated showing a larger sensitivity to fractured rock than P and S velocities taken independently.

The survey can be briefly described as follows:

Source borehole:	F4
Detector boreholes:	F1, F2, F3, F5, F6
Depth range of source:	60 m - 195 m
Depth range of detectors:	60 m -200 m
Depth increment of source:	5 m
Depth increment of detectors:	5 m
Number of rays per section:	appr. 250
Max source-detector distance:	appr. 180 m
Min source-detector distance:	appr. 25 m
Number of sections:	5
Cell size for tomography:	5 m x 5 m
Average P velocity:	6100 m/s - 6500 m/s
Average S velocity:	3600 m/s - 3700 m/s
Average Young's modulus:	88 GPa - 92 GPa

Two lower velocity features of significant extention were found in the volume investigated and were identified as zones "C" and "K". Their positions in the boreholes are:

	Zone "C"	Zone "K"
F1	118 - 132	173 - 183 (165 - 175)
F3	105 - 115	162 - 175
F4	105 - 115 (112 - 123)	160 - 170
F5	92 - 102	145 - 155
F6	110 - 122	155 - 170

1. INTRODUCTION

Seismic tests were performed at the experimental crosshole site in the Stripa mine during the fall 1984 and spring 1985. These tests belonged to the group of 'Crosshole Investigations' together with the radar and hydraulics.

The scope of the crosshole program has been to develop methods for bedrock investigations which can detect fracture zones and determine their position, orientation, size and physical properties. The fracture zones are believed to be the major pathways by which radionuclides could spread away from a spent nuclear fuel repository. The program covered the development of equipment, field routines and interpretation techniques.

The main objective of the crosshole seismic tests has been to study if it is possible to detect by seismic tomography major fracture zones and determine their dimensions and orientation. Another more specific objective was to find out if S waves can be recorded clearly enough to be used with tomographic processing.

The seismic crosshole measurements provide the means to reach with probing instrumentation inside the rockmass. The basic survey procedure is to position a signal source in one borehole and one detector at the same depth in the other hole. The travel time of the wave (P or S) is measured and the seismic velocity is calculated as an indication of the rock quality. Both source and detector are moved with the same depth increment after each measurement is done (Butler and Curro 1981). This method can describe well layered structures when the distance between the boreholes is comparable with the thickness of the layers but is hardly suitable when crystalline rock is concerned. With tomographic surveys, the source location is kept constant while the detector is moved stepwise for each measurement. Then the source is placed to the next location and the detector is moved again along the borehole. The amount of data collected is significantly larger than in the first case. For interpretation the crosshole area is divided in square or rectangular cells and, in principle, all anomalies extending over more than one cell can be correctly positioned.

2. DESCRIPTION OF THE SITE

The Stripa pluton outcrops in a supracrustal belt with structures striking mainly in NE-SW direction. The Stripa granite is grey or reddish, fine to medium grained and it shows relatively dense fracturing on a microscopic scale. The leptite formation surrounding the Stripa granite is a metamorphic product of supracrustal rocks with volcanic origin, which were deposited more than 2000 My ago. The granite at the contact to the leptite occurs partly as inclusions or dikes in leptite.

The test site was situated at the 360 m level of the Stripa mine in a drift where three boreholes had earlier been drilled for hydrological investigations (E1, N1, V1). Six other boreholes were drilled from the end of the drift in a fanlike geometry (F1 through F6 , Fig. 2.1) defining a pyramidal volume extending towards SE. They are currently refered to as the "fan boreholes". The location and orientation of the boreholes are shown in Table 1.1. The rock type at the test site is 'Stripa granite' containing sections of breccias and mylonites. Thin pegmatites, one amphibolite and one aplite sections were also mapped as well as a few quartz veins. The deformed rock has been classified in breccias, mylonites and tectonized rock, where this last category includes all other forms of altered rock (Carlsten et al. 1985).

TABLE 1.1. Position of fan boreholes. Inclination in degrees below horizontal plane, declination in degrees from mine north, length in metres.

	F1	F2	F3
Inclination	10.20	20.57	10.14
Declination	96.25	95.86	106.19
Length	200.10	249.88	199.80

	F4	F5	F6
Inclination	30.96	10.14	40.16
Declination	106.25	122.14	121.92
Length	250.04	200.04	250.05

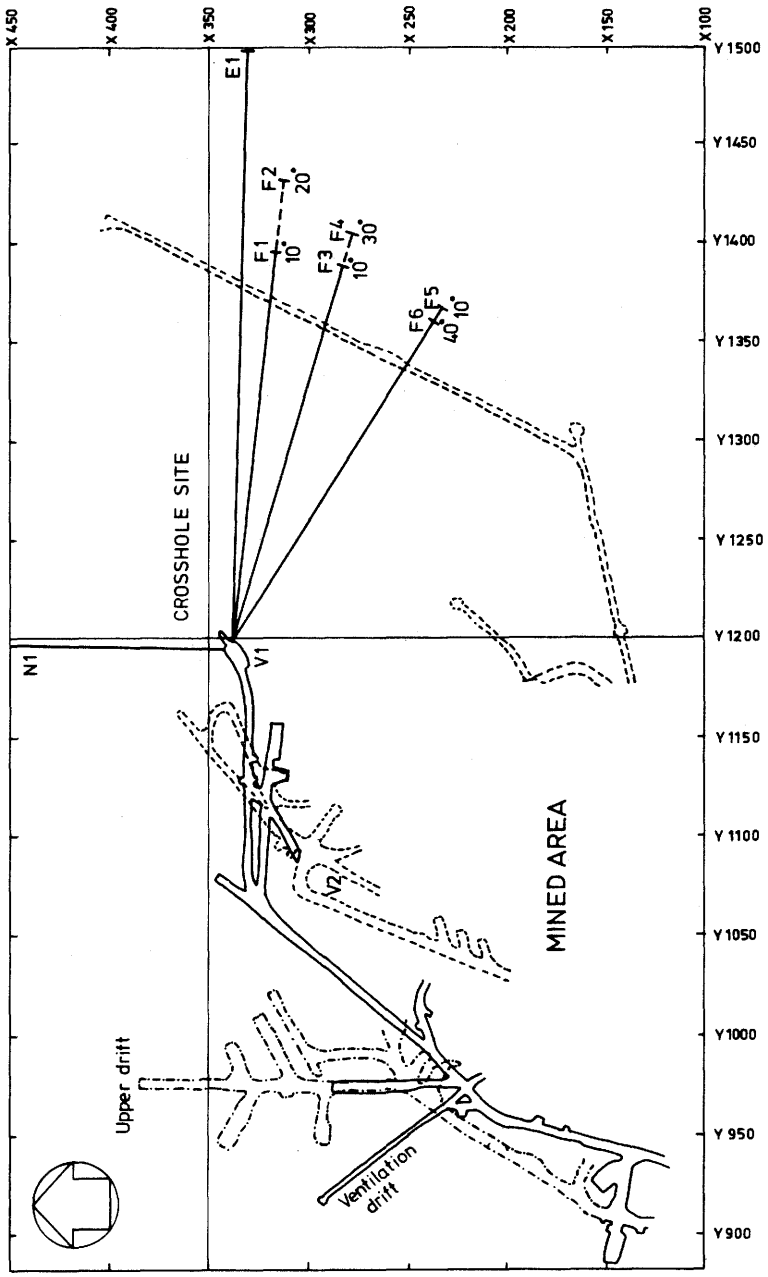

Fig. 2.1 Plan of the Stripa mine levels 360 m and 410 m (dashed line) showing the disposition of the fan boreholes.

The direction of the drilling towards East South-East was chosen following the assumption that the inclined fractures would strike parallelly to the NE-SW orientation of the geological structures. The features detected by the crosshole techniques confirm this assumption. These features consist of combined types of deformed rock, they are red coloured and also display a higher fracture density than the rest of the rockmass.

The main features which could be found by both geophysical (seismics and radar) and hydraulic techniques are (see also Hammarstrom et al. 1986 and Olsson et al. 1986):

Zone "A" intersecting the upper boreholes (F1, F3 and F5) at 35 - 40 m depth,

Zone "C" found between appr. 95 m and 120 m,

Zone "K" located at appr. 160 - 180 m depth and

Zone "L" which does **not** intersect the upper holes but could be detected in F6 at appr. 210 m.

The 'Site Zone' crosses the end of the site drift and was detected by single hole radar but does not intersect the fan boreholes.

Other features were also found by each of the techniques mentioned but probably due to their more local character they were more difficult to correlate and were not included in this description of the site.

The average P wave velocity for competent rock has been found by sonic logging between 6100 m/s and 6500 m/s (Carlsten et al. 1985). These values correlate very well with the seismic crosshole results but seem to differ from measurements elsewhere in the mine. A small but systematic variation was noticed also between the sonic velocity in different boreholes. This indicates that the granitic mass of the site may exhibit seismic velocity variations not connected with fractured zones. This type of variations were outlined also by the crosshole tests, e.g. towards borehole F6.

3. INSTRUMENTATION

The field equipment for these crosshole seismic tests consisted of three main units: the borehole source, the detector probe(s) and the digital seismograph. The data collecting system is shown schematically in Fig 3.1 (Cosma et al 1984).

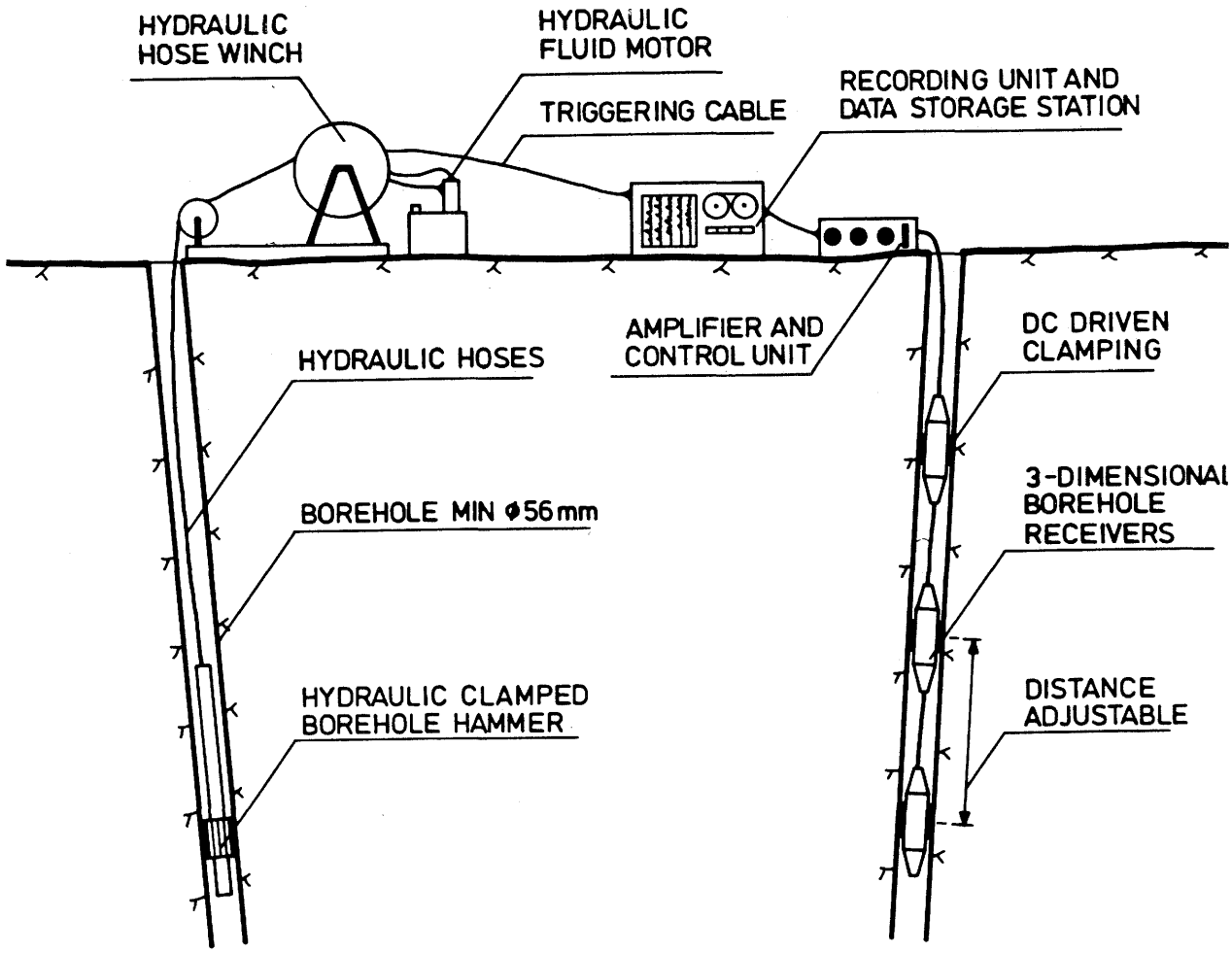

Fig. 3.1 Schematic view of the crosshole system.

3.1. THE BOREHOLE SOURCE

Mechanical shocks were produced in the borehole by a steel hammer sliding inside a waterproof cylindrical enclosure (Fig 3.2). The driving force was provided by a stiff spring which, when compressed and released, moved the hammer along the borehole axis until it hits the end of the cylindrical enclosure. The transmission of energy to the rock was achieved by locking the 'anvil' stricken by the hammer to the borehole wall. The trigger signal for the seismograph was picked up by a pulse sensor placed on the anvil.

The repeated loading and firing of the hammer mechanism as well as the fastening of the anvil to the borehole were done hydraulically. The composite cable attached to the instrument included hydraulic conducts and electrical circuits for the trigger signal and the operation of the down-the-hole valves.

The surface accessories consisted of an electric winch, a hydraulic pump and a command panel. The unit was equipped with a hammer of 2.5 kg delivering 50 J / blow. The blows were repeated at 5-10 second intervals. The stacking was performed at the site directly on the seismograph. The number of measurements added for the same record varied from 5 to 20 and occasionally 40.

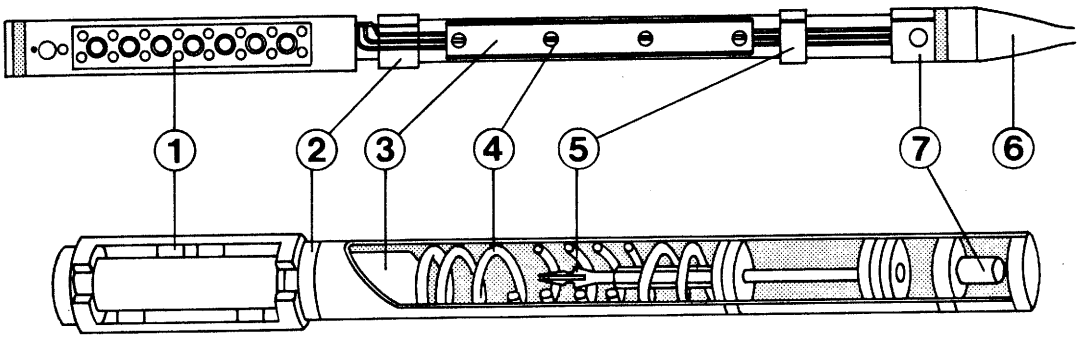

Fig. 3.2 The borehole seismic source. The hammer is housed in the middle section,under the hydraulic loading cylinder. The clamping is achieved by laterally disposed hydraulic cylinders (bottom).

The signal which is output by this device is a transient starting with a high frequecy pulse (8 - 10 kHz) generated by the hammer striking the steel anvil. Lower frequencies (1 - 2 kHz) are present in the coda of the source wavelet being generated by the coupling with the oscillation of the static mass of the enclosure. A signal recorded from an accelerometer attached to the source is presented in Fig. 3.3 (Cosma 1982).

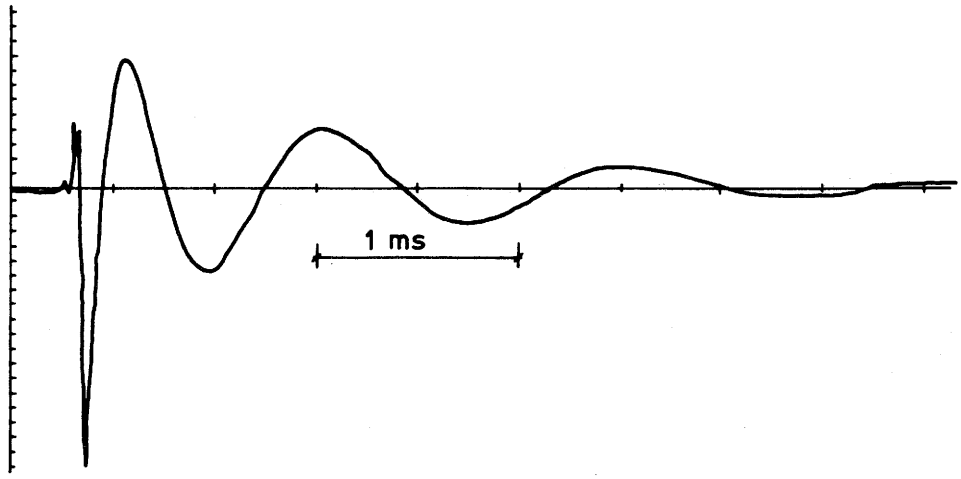

Fig. 3.3 Hammer source signature.

Both P- and S-waves are generated in the rockmass following a dipole-like radiation pattern (Fig.3.4, Heelan 1953). The maximum S wave output is obtained in the transverse direction and theoretically no P wave is output at this angle. The real source gives also a small radial P wave output so that compressional events are always present in the seismograms (Fig. 3.5).

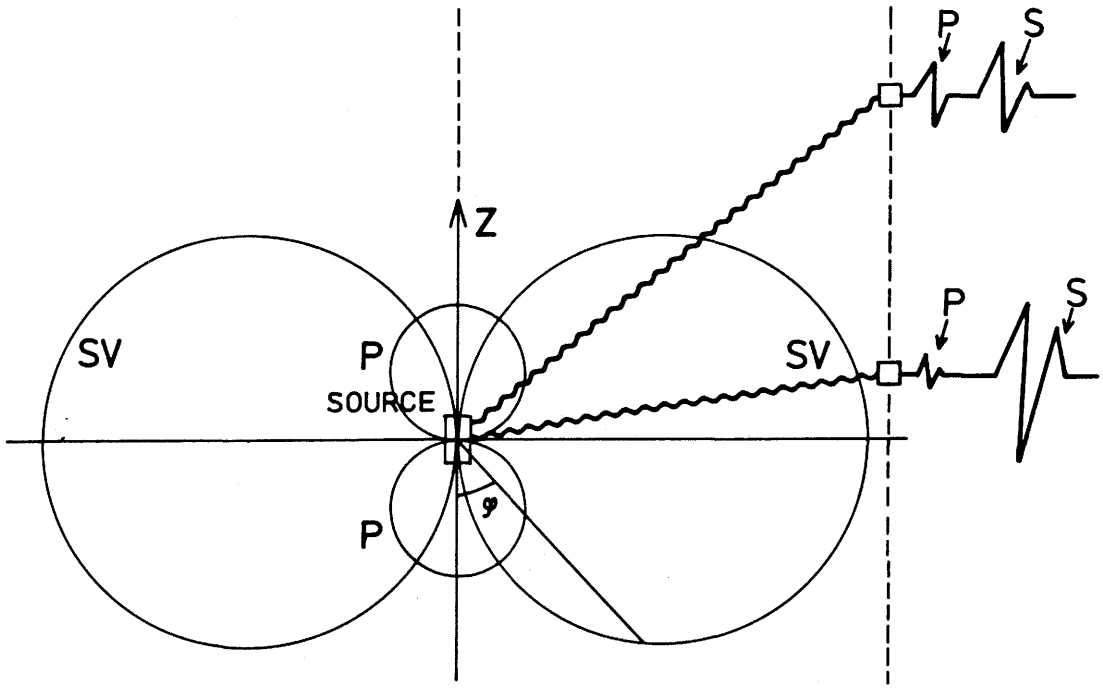

Fig. 3.4 Theoretical radiation pattern of the hammer source. Z is the direction of the borehole (Heelan, 1953).

The repeatibility of the source was checked by stacking more records and monitoring the changes in the signals. Fig. 3.6 shows a pannel starting with 5 and ending with 40 stacked records. The general procedure was to stack 5 hammer shots for each recorded set of seismograms. When a sufficient resolution was not reached, a new series of shots was added so that the total number of stacks would double. It can be seen that the shape of the recorded wavelet stabilises after 5 - 10 pulses. The stability of the source signal is important because the data for tomography is collected by firing the source many times while the interpretation assumes that all signals are recorded from the same source.

3.2. THE DETECTOR PROBE

The detectors consisted of three accelerometers disposed at right angles, preamplifiers and a borehole clamping mechanism driven by an electric motor (Fig. 3.7). The detectors weigh 2.5 kg and they are rated for over 500 m depth under water. Frequencies up to 10 kHz can be used for accurate picking-up of arrival times. Linearity is to be expected up to 5 kHz.

The accelerometers showed a high sensitivity in the KHz range and their ouput is independent of the borehole inclination. Geophones were also tested. Their frequency response was limited upwards around 1 kHz and the time picking accuracy was poorer.

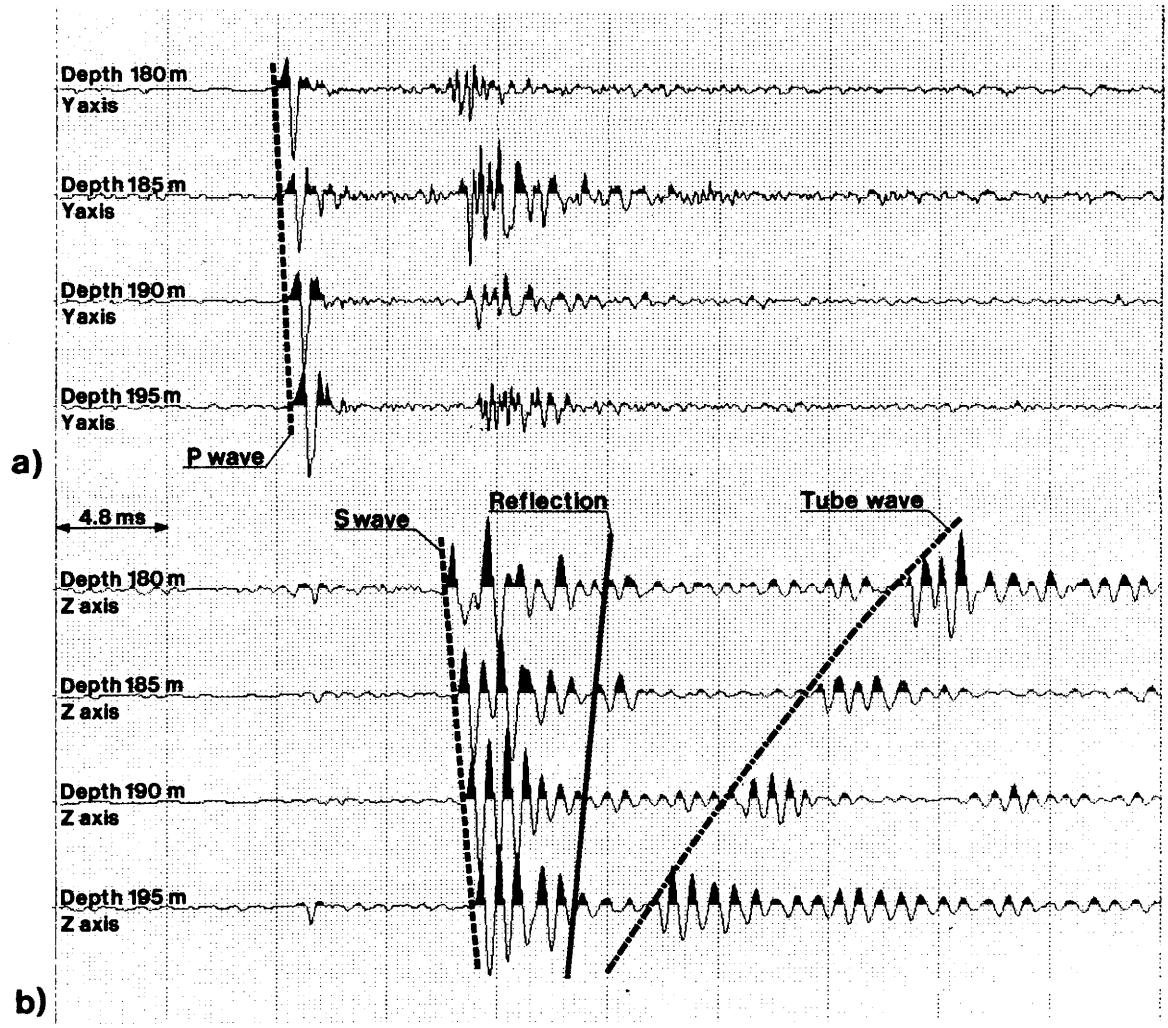

Fig. 3.5 Radial (top) and axial (bottom) signal components recorded at a direction normal to the source.

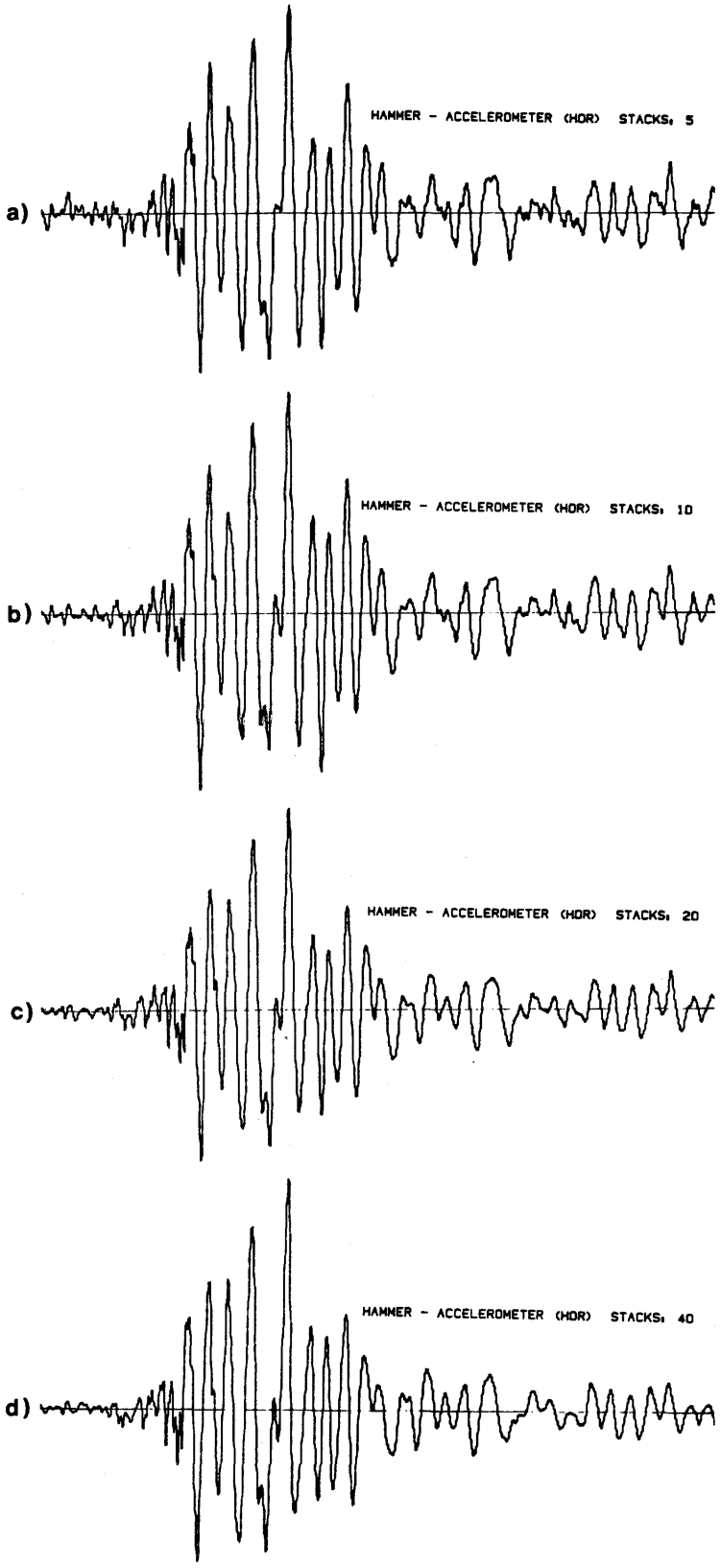

Fig. 3.6 Repeatability test of the hammer source (a: 5 stacks, b: 10 stacks, c: 20 stacks, d: 40 stacks).The shape becomes very stable when more than 10 shots are added. The pulse output by the source (Fig. 3.3) is altered by scattering in the rock.

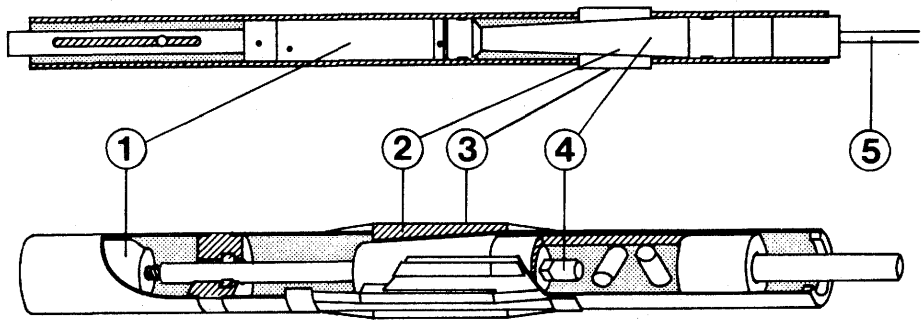

Fig. 3.7 The borehole triaxial detector. The sensors / electronics are placed in the middle / upper part. The clamping parts extend laterally when the outer casing is moved upwards by the electric motor.

3.3. THE DIGITAL SEISMOGRAPH

The ABEM Terraloc unit which was used is a digital 24-channel instrument. It can stack up to 256 measurements on each channel before data transfer to the mass memory. Signals can be displayed before recording on the built-in CRT-monitor and they are stored on tape cassettes. Each channel record is 1000 points long with 8 bits A/D resolution per point. The stacker memory has 16 bit/point resolution. The seismograph also has built-in digital filters and is equipped with a RS-232 serial interface, which was used to transfer the data to computer tapes for processing and storage.

4. FIELD WORK

The field set-up for tomography requires at least two boreholes, one for the seismic source and the other for the detectors. From each source position a fan of 'rays' is emitted towards each detector. Usually this fan is obtained by moving the same detector or a small array of detectors along the borehole and firing the source several times. When one fan is completed the source is moved and the procedure is repeated. When the field work is finished the area between the holes has been scanned in all direction by seismic rays connecting each source to the detectors (Fig 4.1).

The seismic surveys were started in November 1984 at the crosshole site with the equipment described above. The detectors were equipped alternatively with accelerometers or geophones (28Hz,0.11V/cm/s). The accelerometric probes included down-the-hole pre-amplifiers. The signals were passed through extra amplifiers (54 dB) and analog low-pass filters (5 kHz, 5-pole Butterworth). The sampling frequency used through the test was 20 kHz. The source was placed in the borehole F4 and the detectors in each of the other five holes. The sections F4-F6 and F4-F2 were surveyed with geophone probes. Accelerometric probes were used for the other three sections. The step between measuring points was 5 m and recordings were done from every transmitter position to every second receiver position in the following manner:

Shot point No.	Receiving points Nos.
1	1, 3, 5, 7 ...
2	2, 4, 6, 8 ...
3	1, 3, 5, 7 .. .
4	2, 4, 6, 8 ...

The resulting ray net was a superposition of two shifted nets with transmitter step of 5 m and receiver step of 10 m. A more even ray density was thus achieved near the boreholes with less records per unit of depth. The survey was done between 60 m and 200 m in every borehole but only the measurements from 85 to 200 m were used for later processing. Appr. 250 rays were recorded for each section.

More tests were carried out during March 1985. The upper part of the section F4-F6 (30 - 120 m) was surveyed with accelerometers and a higher ray density (5 m steps for the source and 2.5 m steps for the detectors).

The picking-up of the travel times was relatively straight forward for the P-wave as the signal to noise ratio was good and the first event observed in a time series should have been a P wave. The picking-up of the S-wave arrivals was eased by triaxial recording which provided the possibility for polarization filtering. The accurate determination of the S arrivals was occasionally hindered by interference with P multiples and reflections. The procedure for suppressing errors in arrival time picking-up is described in the section 5.3. The accuracy of the arrival times used for tomographic processing is estimated to +/- 0.05 msec. The survey set-up is summarized in Table 4.1.

Table 4.1. Summary of the survey set-up.

Source borehole:	F4
Detector boreholes:	F1, F2, F3, F5, F6
Depth range of source:	60 m - 195 m
Depth range of detectors:	60 m -200 m
Depth increment of source:	5 m (*)
Depth increment of detectors:	5 m (*)
Nr of rays per section:	appr. 250
Max source-detector distance:	appr. 180 m
Min source-detector distance:	appr. 25 m
Number of sections:	5

(*) The measurements were done from every source position to every second detector position. See the text above.

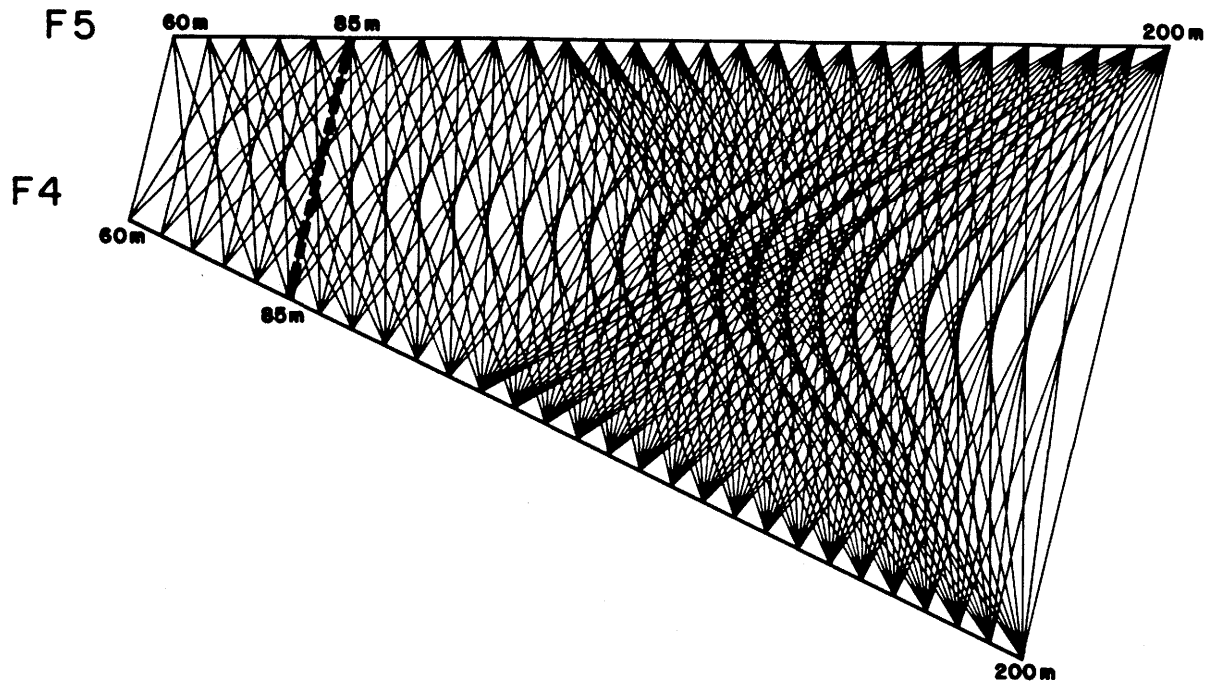

Fig. 4.1 Example of ray coverage of a crosshole sections.

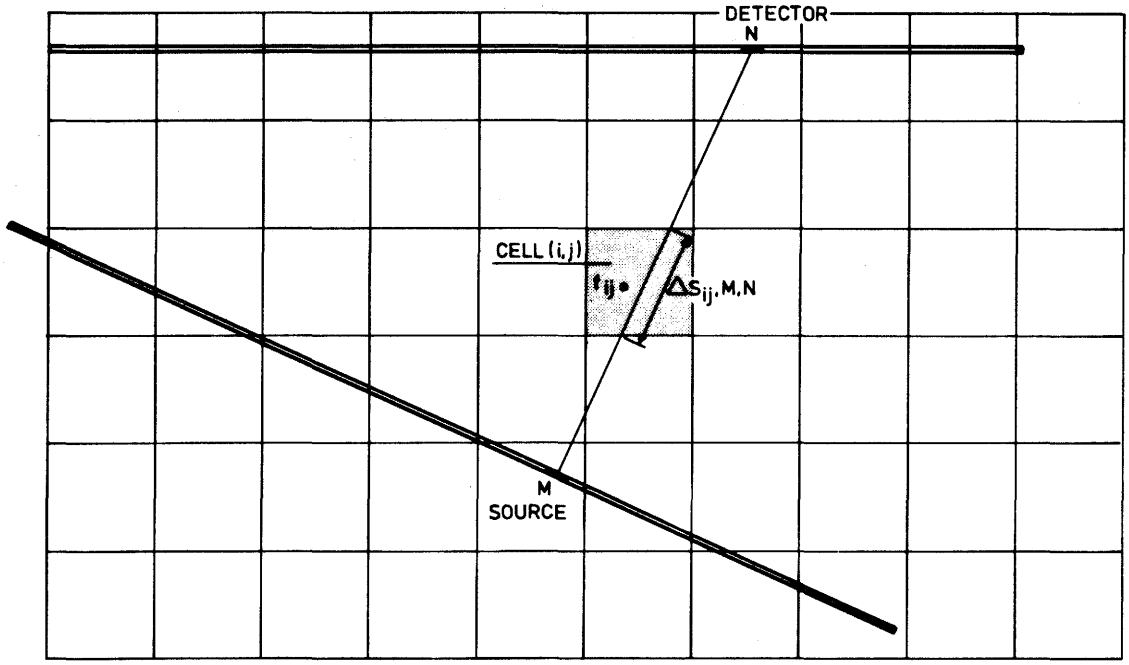

Fig. 5.1 Parametrization of a crosshole section by dividing it in rectangular cells of constant slowness.

5. TOMOGRAPHIC PROCESSING

5.1. THE RECONSTRUCTION ALGORITHM

The velocity distribution between the two boreholes is found by applying an algorithm of the SIRT (simultaneous iterative reconstruction technique) type. A detailed description of the theory of different reconstruction algorithms can be found in Ivansson, 1984. The algorithm which has been used here is derived from Dines and Lytle,1979. Some changes were done to improve the computational speed and the stability of the reconstruction.

With a source at M(x,y) and a detector at N(x,y) the propagation time is given by the integral:

$$t_{M,N} = \int_L f(x,y)\, ds \qquad 5.1$$

where

$$f(x,y) = \left[V(x,y)\right]^{-1} \qquad 5.2$$

is the "slowness" (inverse of velocity).

The space is parametrized by superposing a rectangular grid over the section defined by the boreholes, so that the area is divided in a number of constant velocity cells (pixels), as shown in Fig. 5.1.

The finite linearized expression of (5.1) is

$$T_{M,N} = \sum_I \sum_J F^{I,J} \cdot \Delta S^{I,J}_{M,N} \qquad 5.3$$

where ΔS is the length of the intersection of the ray (M,N) with the cell (I,J).

A simpler form for ΔS is

$$\Delta S^{I,J}_{M,N} = S_{M,N} / K_{M,N} \qquad 5.4$$

where S(M,N) is the total length of a given ray, K(M,N) is the number of cells crossed by the ray. The equation 5.3 becomes

$$5.5 \quad T_{M,N} = \left[S_{M,N}/K_{M,N}\right] \cdot \sum_{I} \sum_{J} F^{I,J} \cdot SIGNUM^{I,J}_{M,N}$$

where SIGNUM(I,J,M,N) is 1 if the ray (M,N) crosses the cell (I,J) and 0 otherwise.

A common practise is to use a 'smoothed' value instead of F(I,J), allowing a certain contribution of the adjacent cells. The smoothing relations act as suplementary equations, creating an over determination of the problem even if the ray coverage is poor or the input data is noisy.

The smoothed value of F(I,J) is given by one of the following two expressions:

$$5.6 \quad \tilde{F}^{I,J} = (G-1) \cdot F^{I,J} + \sum_{i=I-p}^{I+p} \sum_{j=J-r}^{J+r} F^{I,J}$$

or

$$5.7 \quad \tilde{F}^{I,J} = (G-1) F^{I,J} + \left[\sum_{i=I-p}^{I+p} \sum_{j=J-r}^{J+r} F^{I,J} \cdot L^{I,J}\right] \cdot \left[\sum_{I=I-p}^{I+p} \sum_{J=J-r}^{J+r} L^{I,J}\right]^{-1}$$

where p and r give the extent of the smoothing and G is the weight of the central cell. In (5.7) the smoothing is weighted also by L(i,j), the number of rays crossing the adjacent cells. When the structural features with a certain direction are to be emphasized, a form of directional smoothing can be obtained by multiplying F(i,j) in (5.6) and (5.7) with a parameter H(I-i,J-j). The form of H can be chosen so that the weighting is more active in a given direction.

An initial guess is made for F(I,J), e.g. a constant value is confered to the whole field:

$$5.8 \quad F^{o\,I,J} = \bar{F}$$

and propagation times are computed from (5.5).The differences between the measured and computed propagation times are found:

$$5.9 \quad \Delta T^{o}_{M,N} = T^{REAL} - T^{o}$$

The error in apparent slowness is estimated for every ray. The conversion to corrections for the bidimensional field is done by taking the average slowness for all rays crossing the same pixel.

$$5.10 \quad \Delta F^{o\,I,J} = \left[L^{I,J}\right]^{-1} \cdot \sum_{M} \sum_{N} \left[\Delta T^{o}_{M,N} / S_{M,N}\right] \cdot SIGNUM^{I,J}_{M,N}$$

The corrected slowness becomes

$$5.11 \quad F^{1\,I,J} = F^{o\,I,J} + \Delta F^{o\,I,J}$$

and the process is reiterated with the new values. The SIRT method leads to a consistent velcity distribution even if the ray coverage is relatively sparse. However, the contrast obtained in the reconstructed section may be weaker than the actual one.

5.2 PRESENTATION OF RESULTS

The output of the geotomograhy routine is presented as a contrast plot (e.g. Figs 6.1 - 6.5). The intensity of the shade in a given point is a function of the coresponding seismic velocity. Light shades represent high velocities and low velocities are displayed as dark areas. Fracture zones appear as low velocity (dark) features. The grey scale is adjusted automatically to enhance the visual contrast so that the sections may be displayed with different lower and upper limits. The continuity of the velocity boundaries is obtained by dividing the constant velocity blocks in smaller elements and interpolating the velocity values.

5.3 SUPPRESSION OF ERRORS

The crosshole geometry is two dimensional but the boreholes are not expected to lie strictly in the same plane. Therefore, the sources and detectors were projected on a plane representing the closest approximation for the twisted surface containing the two boreholes. The arrival times were corrected according to the alteration of distances. The plane projection of the boreholes does not affect the

quality of the result if the maximum distance from the true measuring points to their projected images does not exceed the transverse continuity of the structure. In this case the deviation of the boreholes from the projection plane was less than 3 m and the transverse continuity of the fracture zones extends far beyond this limit.

Measuring errors may appear when picking up the arrival times. Tomography is very sensitive to these errors and one wrong measurement is enough to alter the general appearence of the result. It is practical to exclude from the tomographic processing the unclear arrivals and to perform the reconstruction only with the accurate data. With a sufficient number of measurements the result is not influenced by eliminating a few rays. For example the difference between two synthetic error free velocity distributions obtained with 200 rays and 250 rays could not be noticed in the contrast plots. Therefore, the noisy signals containing poorly defined arrivals were not used.

Another way to suppress measuring errors was to plot the residual misfit for each ray after running the tomographic program for a few iterations. The measurements displaying distinctively high errors were excluded.

Even if the onset is clear, the beginning of the signal is not easy to point out just from the amplitude level. Other criteria used for enhancing the resolution of the measured times were frequency, phase, polarization and coherence. Each triaxial signal was compared with the signals originating from the two nearby source positions and reaching the two adjacent detectors. The frequencies present in a window containing the estimated arrivals for each of these signals were used for defining band-pass filters. The onsets displaying a polarization along the raypath (for P arrivals) or normal to the ray path (for S arrivals) were enhanced by an elliptical normalization function. Finally, a covariance operator was applied in the time window mentioned above to enhance the wavelets with similar shapes. This procedure led to a more consistent evaluation by using the information contained in the whole wavelet associated with the arrival. However, the times determined in this way contain an offset of appr. half of the main period of the wavelet.

The time offset and the errors in source and detector positions, which become more important with increasing depth, may produce an effect similar to anisotrophy. The correction was done by following the dependence of the velocity of each ray with the angle of shooting and depth. The presence of the offset and positioning errors could be noticed in the velocity distribution matrix as a cross-like artifact. In a polar diagram of the velocity vs. the ray angle the error free distribution should closely follow a circle. In reality the longer diagonal rays are less affected by errors while the shorter ones connecting sources and detectors at the same depth are assigned a significantly altered velocity. Consequently an ellipse fits the angular distribution better than a circle.

The first step of the correction is to find the ellipse which best approximates the angular variation of all velocities measured in one section. The coordinates of each point V1 (Fig. 5.2.a) will be compensated so that the exentricity of the ellipse becomes 1. The fit for the angular distribution becomes then a circle (Fig. 5.2.b) which means that the mean velocity is now the same in all directions.

This process allows the ratio between the velocities of two rays shot at the same angle but from different positions to remain constant. A ray crossing a fracture zone will therefore display lower velocity also after the transform. The second step of the procedure is to adjust the radius of the circle so that both short and long rays are assigned the same average velocity. This is done by substacting from each travel time the mean offset (Fig. 5.2.c).

The assumed straight path from source to detector is an approximation as the rays bend due to the uneven velocity distribution through the section. An algorithm for computing in two dimensions the path of the seismic rays was applied but without bringing any noticeable improvement. The small velocity differences through the whole site did not cause important ray bending and the straight ray approach was found acceptable.

If no equations are available except (5.3) the number of pixels cannot exceed the number of measured propagation times. If this condition were to be observed the size of the constant velocity areas would be large and the artificial discontinuities introduced would hinder the convergence of the reconstruction procedure. A relatively dense parametrization was used at Stripa (pixel size: 5 m x 5 m) giving a larger number of pixels to be resolved than measured times. The subdetermination

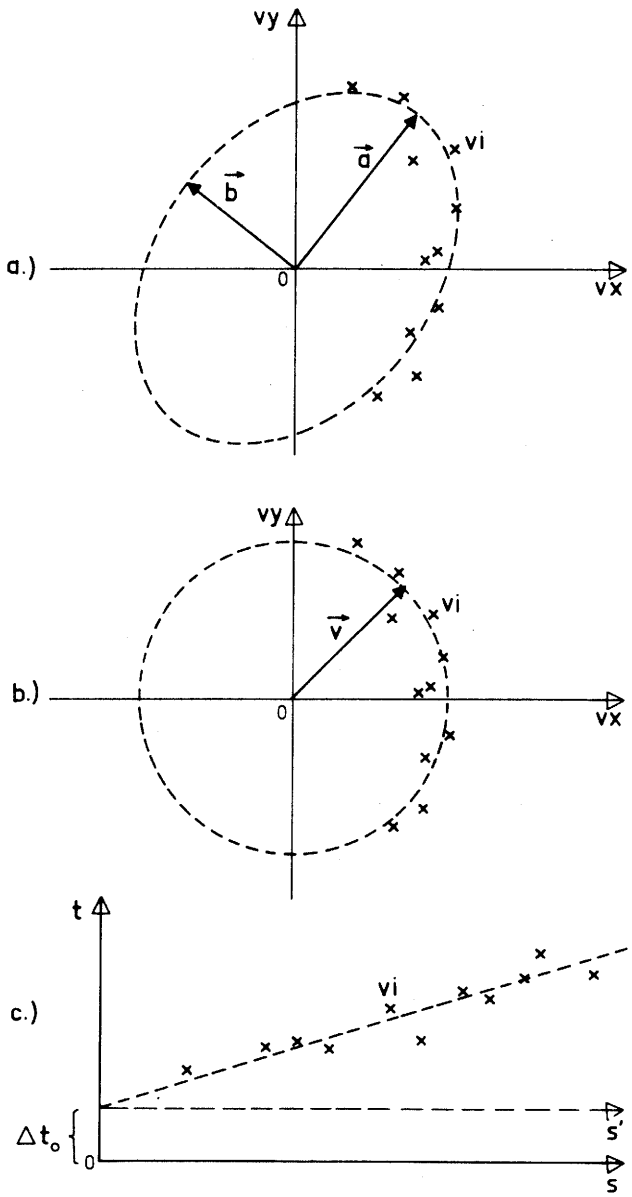

Fig. 5.2 Corrections for elliptical velocity disrtibution and time offset (y axis is along the bisectrix of the section).

a. Angular distribution of measured velocities.
b. Distribution corrected for position offset.
c. Correction for time offset.

of the system of equations was compensated by smoothing the velocity matrix between iterations. This helped to follow more closely the continuous velocity variations. The smoothing was weighted by the number of rays crossing each pixel so that the elements containing more rays influenced the average to a greater extent than the surrounding less scanned elements.

The resolution is lower at the top and at the bottom of the sections as relatively few rays cross these areas and they are nearly parallel. Errors tend to accumulate in these zones as 'artifacts'.

6. RESULTS

The description of fracture zones as linear (planar in 3-D) features is an abstraction. In reality the physical properties of the rock vary from point to point along the same feature. Generally, one has to enhance the linearity of the features to make interpretation possible. For example the reflection methods would not be applicable if one did not start from a zero-order planar model.

The tomographic technique does not use apriori assumptions regarding the structure to be resolved. Moreover, tomography operates with areas and not with defined objects and tends to smear out the features, would they be linear or not, into ellongated spots. It follows then that the tomographic contrast plots can be interpreted in terms of position and orientation of fracture zones but the algorithm itself does not make any discrimination between features with clear geometry and local irregular velocity anomalies. When refering to linear features in the following discussion we actually idealize the geometry so that we can compare the results with the information obtained by other methods.

The sections F4-F1 and F4-F3 were reconstructed for both P and S velocities. Although the two travel times sets are obtained from the same seismograms they are essentially independent. The features displayed in both cases are concordant with each other and also concordant with the information available from the other surveys performed at the crosshole site.

We have also computed as an exercise the dynamic Young's moduli from the corresponding P and S velocities with the sources and the detectors placed at equal depths (Figs. 6.1.a and 6.1.b). The density of the rock was assumed to be constant (2800 kg/m3). The values of the elastic parameters follow the positions of the fractured zones as infered from tomographic processing. Zones "C" and "K" leave clear marks on the moduli plots and the moduli curves are much more sensitive to differences in rock quality than the corresponding P and S velocity curves.

This way of processing cannot define the orientation of the fracture zones but their presence can be detected as a preliminary exercise, before tomographic processing. The rockmass quality is better expressed quantitatively by the elastic parameters than by the seismic velocities.

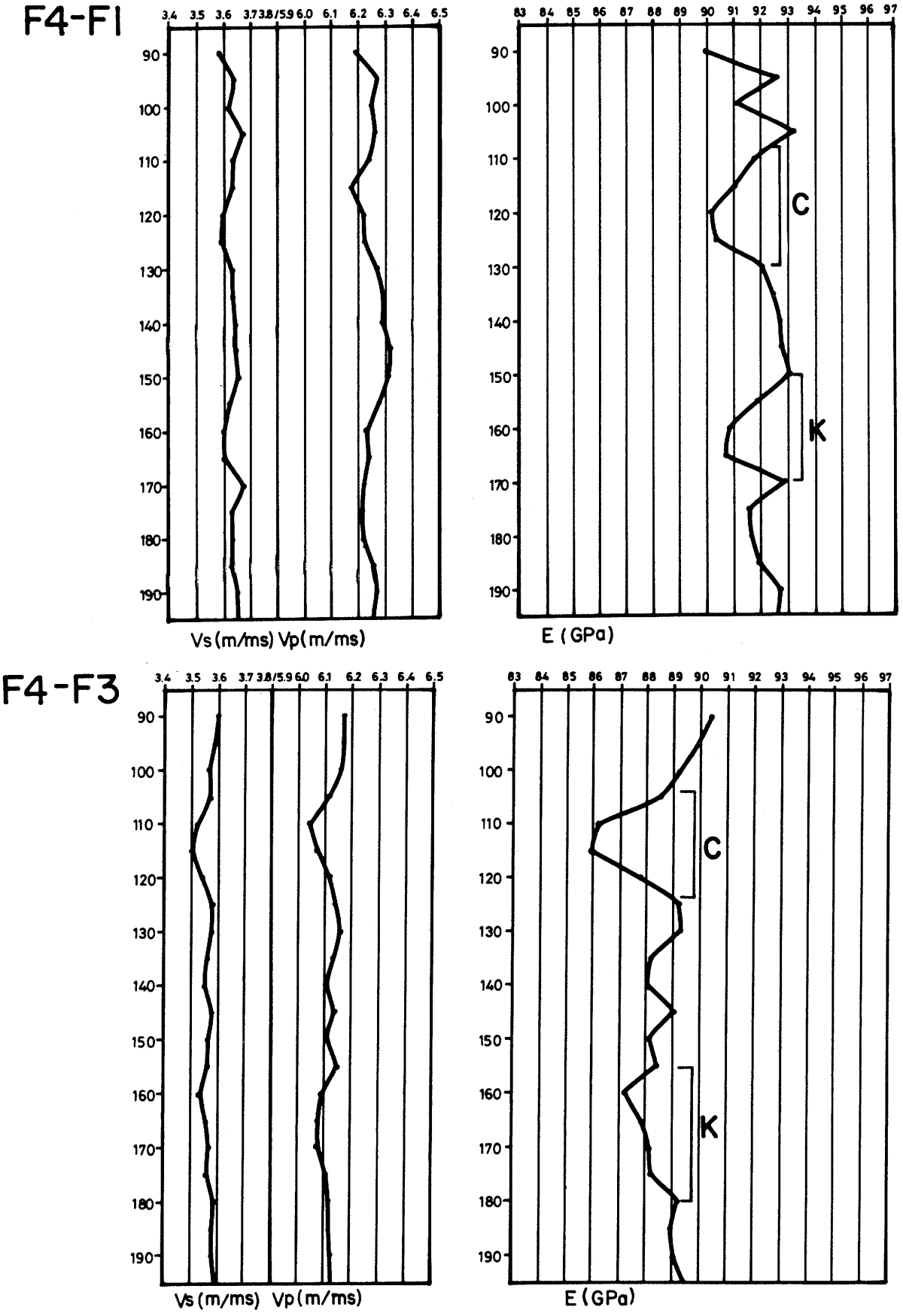

Fig. 6.1 Velocity vs. depth diagrams (left) and Young's modulus vs. depth diagrams (right). Zones "C" and "K" are clearer in the modulus curves than in the P and S velocity ones.

The low spread of the Young's moduli is an indication of the homogeneity and good quality of the Stripa granite.

The overall velocity contrast through the whole surveyed volume was remarcably low. In the section F4-F5, 90 % of the measured velocities are between 6100 m/s and 6200 m/s. The spread is slightly higher in the other sections. The magnitude of the combined effect of the positioning and time offset errors (appr. 2 - 4 %) was comparable with the overall contrast and had a strong influence on the resolution.

After correction more or less linear low velocity features appeared clearly in all sections surveyed by acceleometers. Zones "C" and "K" which intersect the fan boreholes within the surveyed depth range were positively identified. Zones "A" and "L" are outside this range. The drift crossing at the 410 m level was also found.

Table 5.1. shows the positions in the boreholes of the zones "C" and "K" as they have been found by seismic tomography.

TABLE 5.1. Depths (m) of zones "C" and "K" in the fan boreholes.

	Zone "C"	Zone "K"
F1	118 - 132	173 - 183 (165 - 175)
F3	105 - 115	162 - 175
F4	105 - 115 (112 - 123)	160 - 170
F5	92 - 102	145 - 155
F6	110 - 122	155 - 170

Zone "C" responds to all investigation methods applied at the crosshole site. Geologically it was described as strongly tectonized and brecciated. The fracture density is in average relatively high but varies widely in different boreholes. This zone is also one of the most hydraulically conductive.

Reflection radar and seismic tests show that zone "C" bifurcates in at least two nearly parallel subunits. Tomography does not detect the bifurcation directly, the reasons being explained in the beginning of this section, but shows variations in the thickness of the zone.

Zone "K" was not described as a separate unit by single hole surveys, probably due to its irregular character. Reflection radar tests detected it but it seems difficult to assign to this zone unambiguous values for dip and strike.

It may well be that geologically this zone is formed by the contribution of units "E" and "F" (Carlsten et al. 1985) but within the volume of the site it appears as a series of low velocity features which connect some of the assumed borehole intersections of units "E" and "F".

The quality of the tomography output was better for the three sections investigated by accelerometric probes (F4-F1, F4-F3 and F4-F5). The section F4-F2 which was surveyed with geophone receivers, gave unrealiable results and this section was not included in the interpretation. The section F4-F6 was obtained by combining the geophone results from the first set of field tests with the accelerometric measurements done later for the upper part of the section. The rays recorded both with geophones and accelerometers were used for cross-calibration. Qualitatively the velocity distribution is correct but the section displays higher mean velocity and reconstruction error than the three sections surveyed only by accelerometers.

6.1. SECTION F4 - F1

Zone "C" is clearly visible in the P wave reconstruction (Fig. 6.2.) between 105 - 115 m in F4 and 118 - 132 m in F1. The widening of zone "C" towards F1 could contain also the feature recognized earlier as zone "D" or more likely a bifurcation of zone "C". Zone "K" gives a parallel mark to "C" intersecting F4 at 160 - 170 m and F1 between 173 and 183 m. The tunnel at the 410 m level crossing the section near the bottom can also be seen.

The reconstruction based on S-velocities (Fig. 6.2) displays basically the same features but the resolution is lower. This is due to the difficulty of measuring accurately the travel times of S waves. Zone "C" is placed in F4 lower than in the P wave plot, at 112 - 122 m.

6.2. SECTION F4 - F3

In the P wave plot (Fig. 6.4) zones "C" and "K" intersect F4 at 112 -122 m and 160 -170 m, which agrees with the previous S wave section. In F3 zone "C" crosses at 105 m - 115 m and zone "K" at 162 - 175 m. Another feature, probably of a more local character, appears in F4 at 130 - 140 m slanting towards the bottom. Although this feature leaves

similar marks on both P and S velocity reconstructions, it cannot be unambiguously found in the other tomographic sections. A possible explanation is, that the tomography is most sensitive to features perpendicular to the bisectrix of a given section. If the same feature itersects other sections at a steep angle it might remain undetected. The 410 m tunnel appears in its correct position. The S wave plot (Fig. 6.5) shows the same features and it is apparent that a planar "K" zone could not explain the pattern at the bottom of the picture. As said above, zone "K" has been described as discontinuous also by the other investigations.

6.3. SECTION F4 - F5

The velocity contrast in this section is extremely low, close to the limit of resolution (Fig. 6.6). Zone 'C' crosses from 105 - 110 m in borehole F4 to 92 - 102 m in F5 and shows a discontinuity in the middle of the section. Zone 'K' extends as a sequece of darker spots between 160 - 170 m in F4 and 145 - 155 m in F5. The tunnel leaves an elongated mark under zone "K" and part of zone "L" appears in F5 in the lower left corner.

6.4. SECTION F4 - F6

This section has the highest mean velocity and also the largest average reconstruction error probably due to the combination of accelerometric and geophone data.

Zone "C" extends from 105 - 115 m in F4 to 110 - 122 m in F6 (Fig. 6.7). Zone "K" is apparent at 160 - 170 m in F4 but gradually vanishes towards F6. Its extrapolated depth in F6 would be 155 - 170 m.

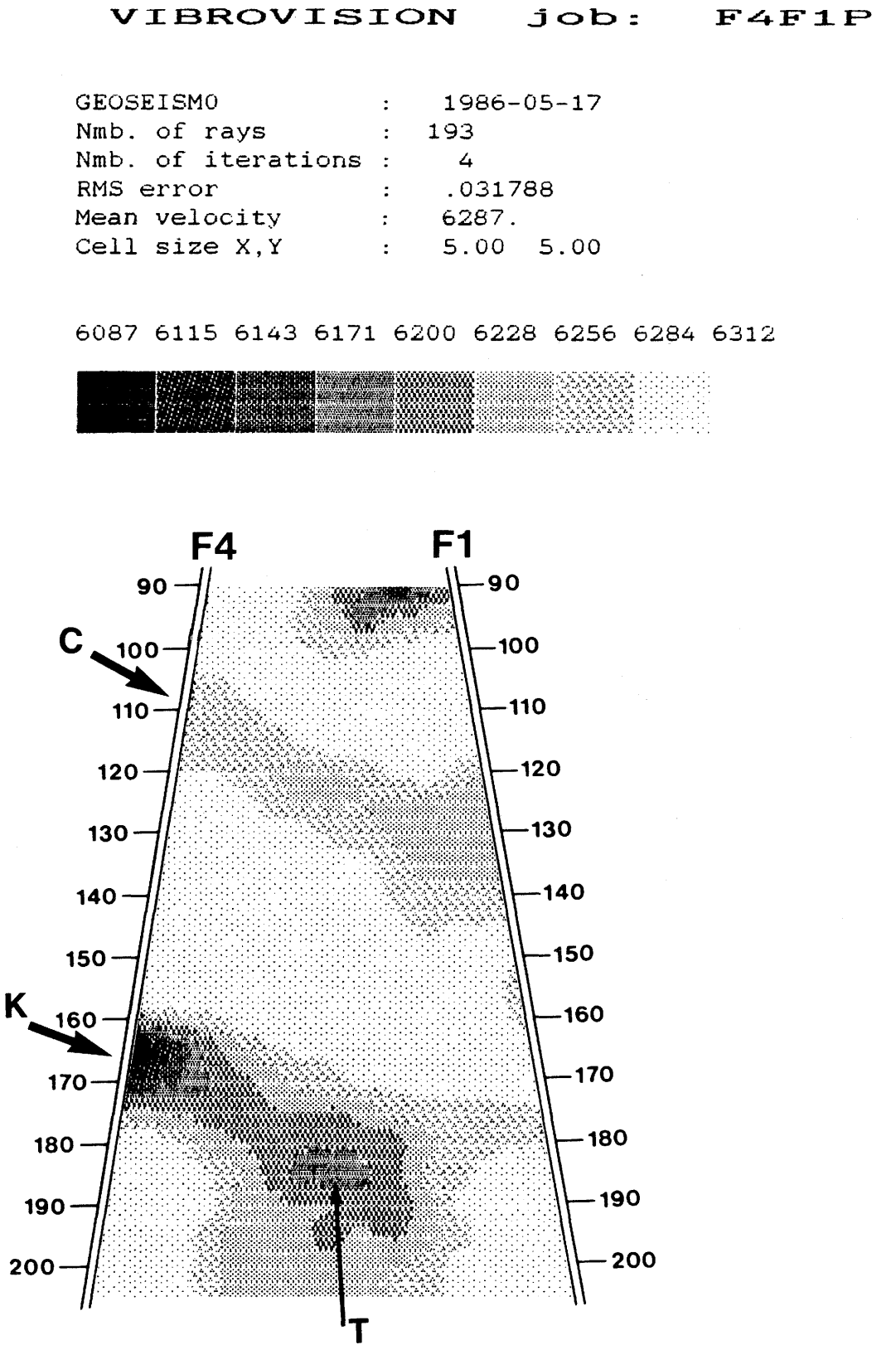

Fig. 6.2 P wave tomographic reconstruction of section F4 - F1.

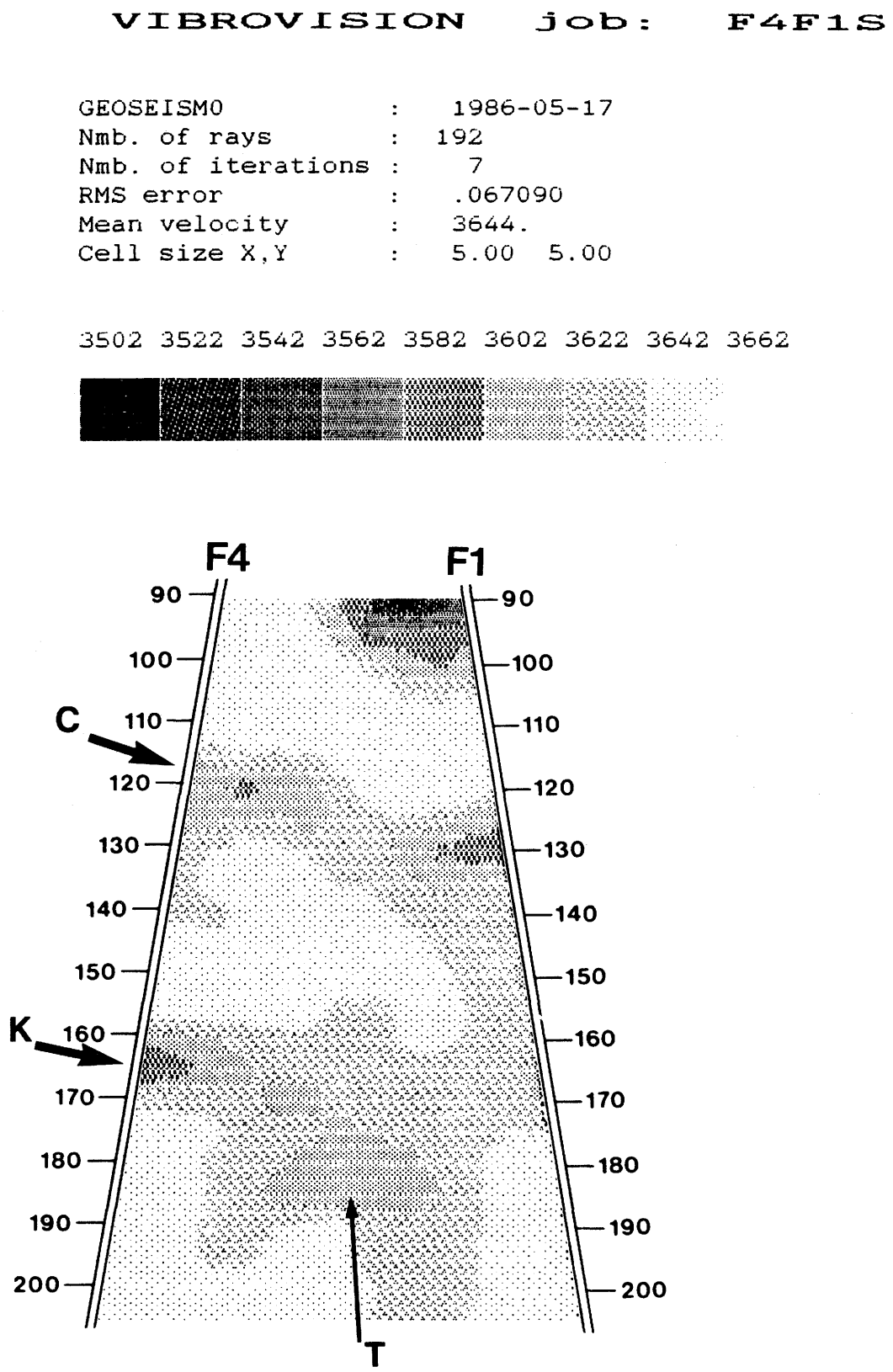

Fig. 6.3 S wave tomographic reconstruction of section F4 - F1.

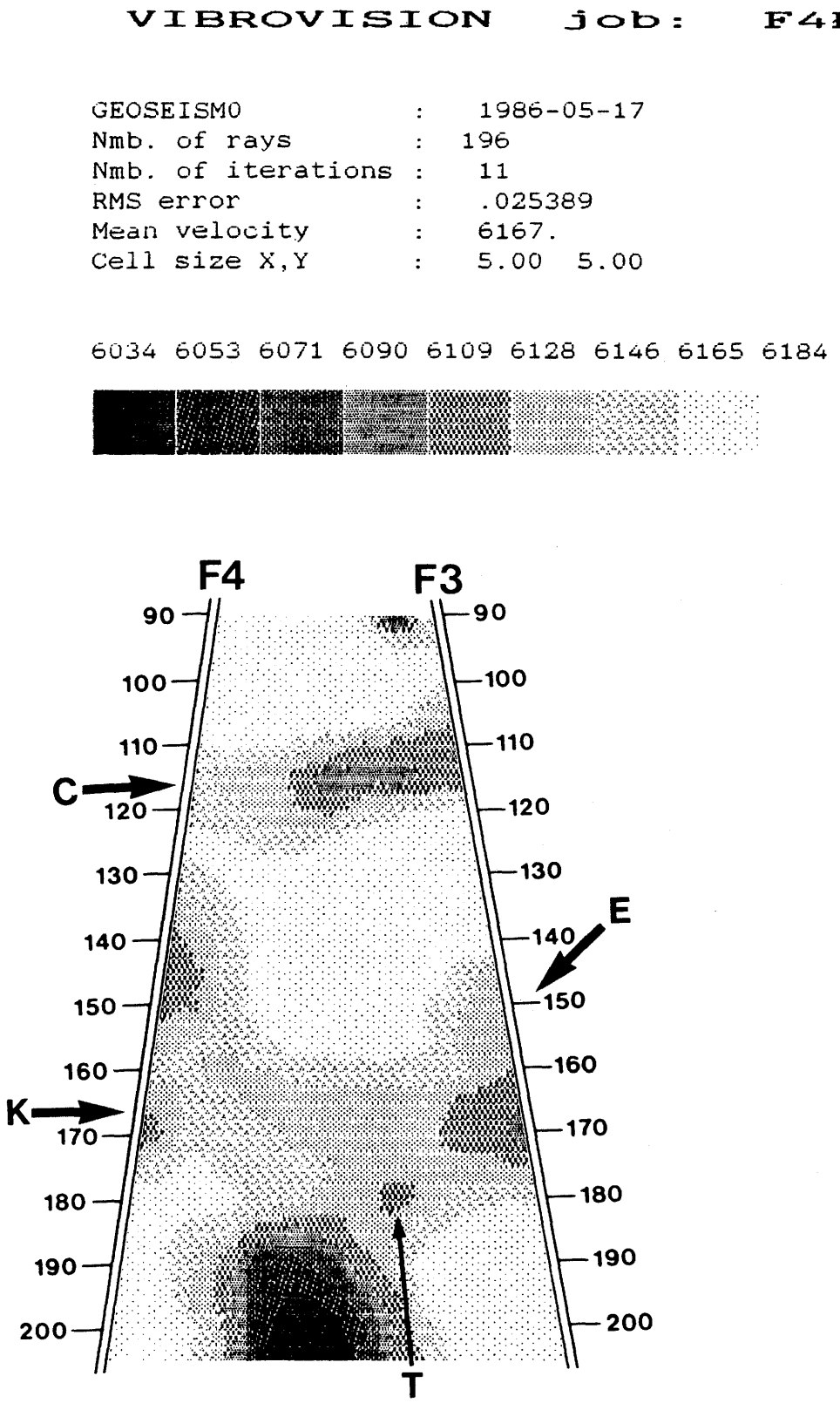

Fig. 6.4 P wave tomographic reconstruction of section F4 - F3.

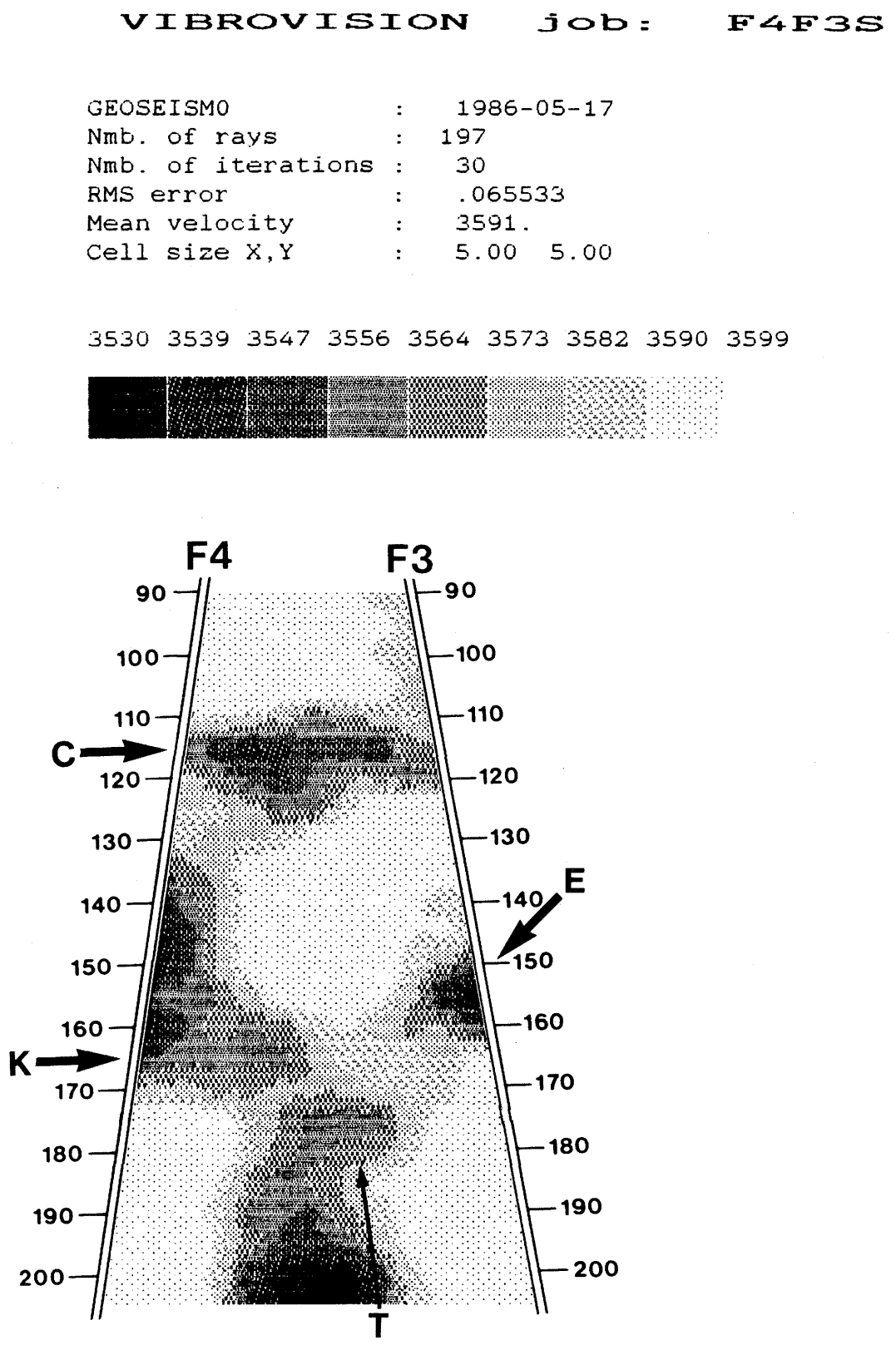

Fig. 6.5 S wave tomographic reconstruction of section F4 - F3.

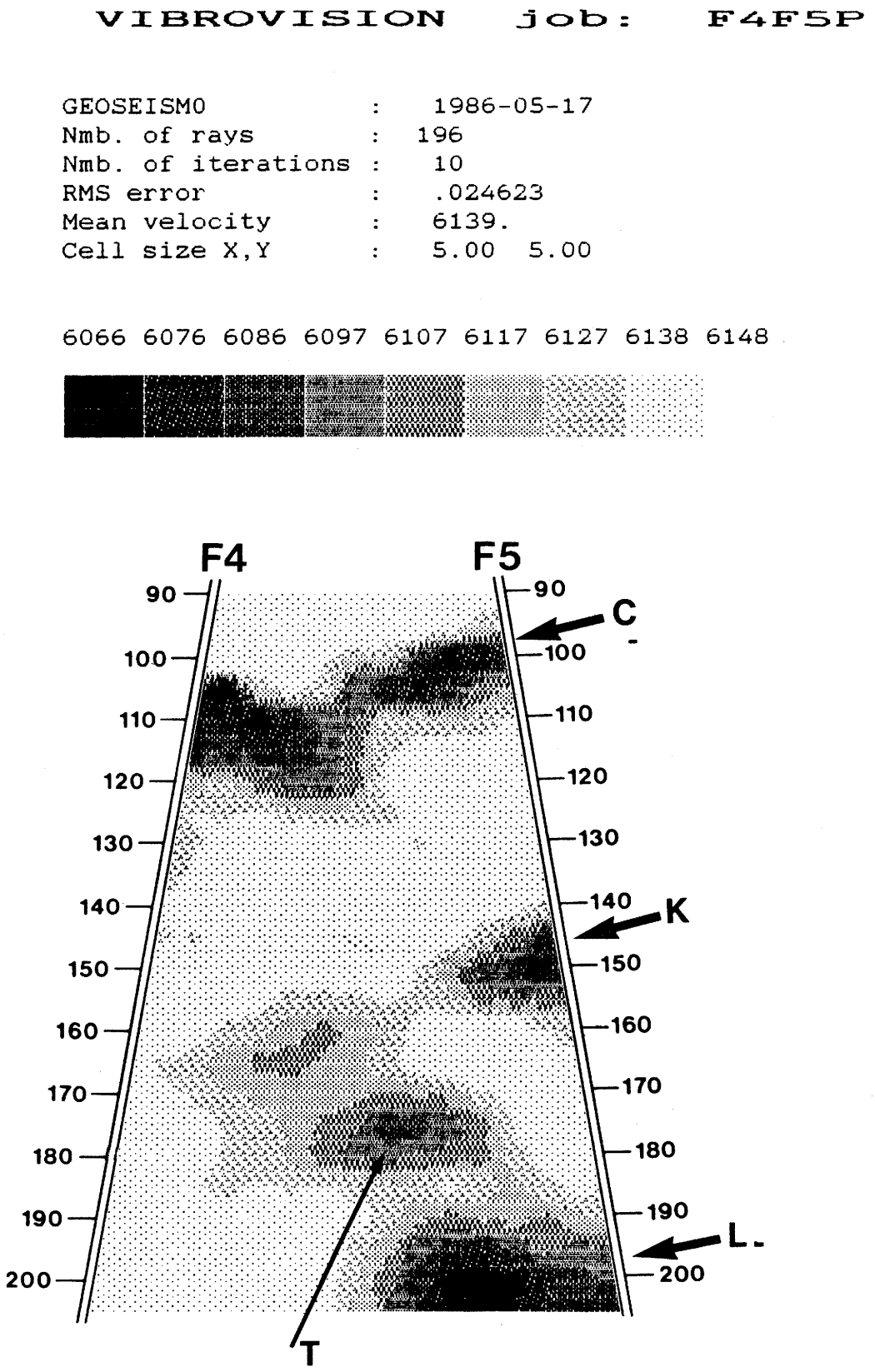

Fig. 6.6 P wave tomographic reconstruction of section F4 - F5.

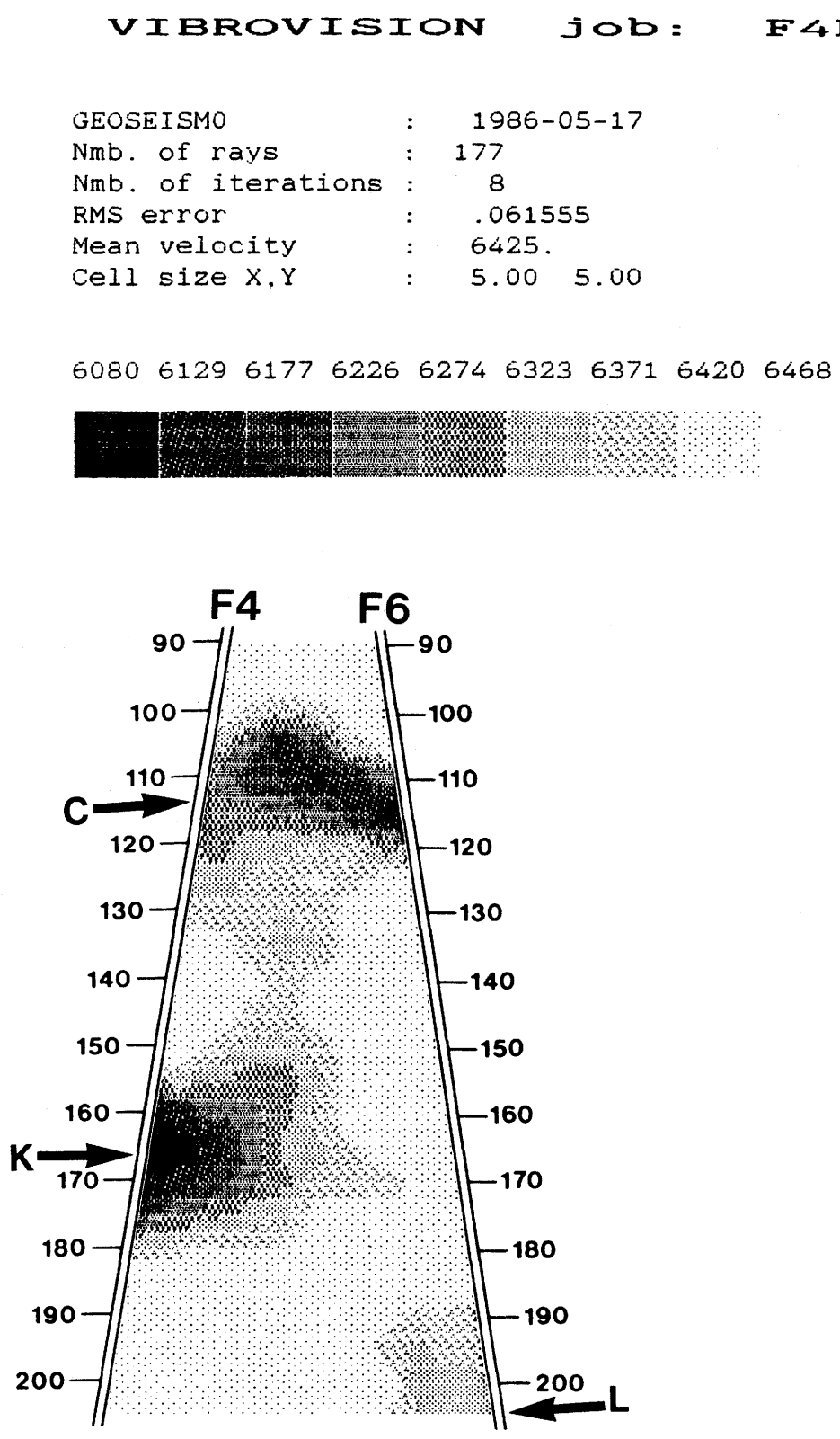

Fig. 6.7 P wave tomographic reconstruction of section F4 - F6.

7. CONCLUSIONS

The tomographic sections obtained by crosshole seismics describe two main features earlier identified as zones "C" and "K". Tomography could give a clear picture of how these features connect between the boreholes.

The fracture zones are not strictly planar within the range of tomography and their thickness and mechanical properties vary across the section. Discontinuities and local anomalies have been noticed.

By combining the information from all sections the position of the observed features could be defined in three dimensions. Both of them are subvertical and strike NE-SW.

The results obtained from P and S waves are in good agreement with each other but the S wave velocity distributions display a higher noise. The processing of both P and S velocities gave more confidence in the interpretation of the structures.

The tomographic technique was found to be very sensitive to noise in the input data and several precautions had to be taken in order to get an unambiguous result. The position of the boreholes and the travel times were determined with great accuracy but even so the the program had to be adjusted to compensate the small remaining errors. This fine tuning of the program is as important as the reconstruction algorithm itself and consistent results could not be obtained without it.

The equipment performed well and the field work was carried out without technical problems. The mechanical source produced repeatable seismic pulses which could be recorded clearly through the whole range of the tests (appr. 200 m). Some details in the construction of the detectors have to be altered in order to achieve a better coupling to the borehole also at frequencies over 5 kHz. With this application the accelerometers were clearly superior to the electrodynamic pick-ups (geophones). The advantages of the recording system used were its special design for rough field conditions and the uncomplicated operation. The main short-coming was the only 8 bit A/D resolution.

The general conclusion of these tests is that seismic tomography can be applied successfully to the detection of fracture zones in crystalline rock. The geometry of the fractured zones is more confidently defined by combining the results of tomography with reflection data.

8. REFERENCES

1. Butler, D. and Curro, J. "Crosshole Seismic Testing - Procedures and Pitfalls", Geophysics, v. 46, pp. 23-29, 1981.

2. Carlsten, S., Magnusson, K-A., Olsson, O. "Crosshole Investigations, Description of the Small Scale Site", Stripa Project, Internal Report 85-05, KBS Stockholm, 1985.

3. Cosma, C. "Crosshole Seismic Investigations", The Finnish Association of Mining and Metallurgical Engineers, Serie A Nr. 67, 1982.

4. Cosma, C., Ihalainen, M., Korhonen, R. "Crosshole Seismic Method", The Finnish Association of Mining and Metallurgical Engineers, Serie A Nr. 73, 1984.

5. Hammarstrom, M., Ivansson, S., Moren, P., Pihl, J. "Crosshole Investigations, Results from Seismic Borehole Tomography", Stripa Project, Report, 1986.

6. Heelan, P. A., "Radiation from a Cylindrical Source of Finite Length", Geophysics, v.18, pp. 685-696, 1953.

7. Ivansson, S. "Crosshole Investigations, Tomography and its Application to Crosshole Seismic Measurements", Stripa Project, Internal Report, SKB, 1984.

8. Olsson, O., Falk, L., Forslund, O., Lundmark, L., Sandberg, E. "Crosshole Investigations, Results From Radar Investigations", Stripa Project, Report, 1986.